Microelectronics Journal ▮ (▮▮▮▮) ▮▮▮–▮▮▮

Contents lists available at ScienceDirect

Microelectronics Journal

journal homepage: www.elsevier.com/locate/mejo

Development of an FPGA-based system for real-time simulation of photovoltaic modules

Eftichios Koutroulis *, Kostas Kalaitzakis, Vasileios Tzitzilonis

Department of Electronic and Computer Engineering, Technical University of Crete, Campus, GR-73100 Chania, Crete, Greece

ARTICLE INFO

Article history:
Received 14 March 2007
Received in revised form
5 March 2008
Accepted 21 May 2008

Keywords:
Photovoltaic system
Simulator
DC/DC converter
Field programmable gate array
Rapid system prototyping

ABSTRACT

Photovoltaic (PV) simulators are indispensable for the operational evaluation of PV energy production system components (e.g. battery chargers, DC/AC inverters, etc.), in order to avoid the time-consuming and expensive field-testing process. In this paper, the development of a novel real-time PV simulator based on Field Programmable Gate Arrays (FPGAs), is presented. The proposed system consists of a Buck-type DC/DC power converter, which is controlled by an FPGA-based unit using the Pulse Width Modulation (PWM) principle. The system operator is able to define both the PV module type to be simulated and the environmental conditions under which the selected PV module operates. The proposed design method enhances the rapid system prototyping capability and enables the reduction of the power converter size and cost due to the high clock speed feature of the FPGA-based control unit. The experimental results indicate that, using the proposed method, the PV module current–voltage characteristics examined are reproduced with an average accuracy of 1.03%.

1. Introduction

Photovoltaic (PV) simulators are power electronic systems capable to reproduce the current–voltage (I–V) output characteristics of PV modules. They are indispensable for the operational evaluation of PV energy production system components such as battery chargers, DC/AC inverters, maximum power point tracking systems, etc. [1], thus aiming towards the rapid prototype development of the corresponding devices, since the field-testing process is expensive, time-consuming and depends on the weather conditions. Additionally, using PV simulators, the PV energy production calculations performed prior to the PV modules installation at the site under consideration, are more accurate and flexible to changes, thus increasing the target power supply system reliability with reduced cost and failure risk.

Several methods of PV simulators have been suggested such as modifying a voltage source so that its internal resistance varies exponentially with the output current [2,3], or amplifying the voltage and current of a low power reference solar cell, which is illuminated by a DC halogen lamp in order to emulate the incident solar irradiance [4]. The PV simulator presented in [5], is based on the amplification of a p–n photosensor output voltage by a DC power amplifier. A similar design method is presented in [6]. A class-A power amplifier is used to amplify the command current or voltage values stored in an EPROM, which correspond to the simulated PV module I–V characteristic. In [7], a voltage-regulated DC power supply with adjustable current-limit setting and a resistor switched by a control circuit according to the Pulse Width Modulation (PWM) principle are employed in order to implement a nonlinear power source simulating a PV panel. Common disadvantage of these methods is that the developed PV simulators are not flexible to changes in case that different PV module types or PV module configurations are simulated. Additionally, the system operator is not able to define the accurate temperature and solar irradiance operating conditions of the simulated PV module, which highly influence the PV module operation.

Microcontroller-based PV simulator implementations are presented in [8–11]. The PV module mathematical model included in the microcontroller program is used to control a power converter, which is usually of switched-mode type in order to achieve high-energy conversion efficiency. In a similar method, presented in [2,12] the PV simulator consists of a switching power supply, which is controlled using a PC according to the PV module mathematical model included in the computer control algorithm. The operation of the PV simulator presented in [13] is based on the control of a power converter according to an algorithm executed by a PC based on measurements of the simulated PV module I–V characteristic. Using these digital PV simulator

* Corresponding author. Tel.: +30 28210 37233; fax: +30 28210 37542.
E-mail address: efkout@electronics.tuc.gr (E. Koutroulis).

0026-2692/$ - see front matter © 2008 Elsevier Ltd. All rights reserved.
doi:10.1016/j.mejo.2008.05.014

Please cite this article as: E. Koutroulis, et al., Development of an FPGA-based system for real-time simulation of photovoltaic modules, Microelectron. J (2008), doi:10.1016/j.mejo.2008.05.014

implementations various PV modules types can be simulated, while simultaneously the temperature and solar irradiance operating conditions of the simulated PV modules can be modified in real-time.

The development of a novel real-time PV simulator, based on Field Programmable Gate Arrays (FPGAs), is presented in this paper. The proposed simulator consists of a switched-mode, step-down (Buck-type) DC/DC power converter, which is controlled by an FPGA-based unit using the PWM principle, in order to reproduce the output voltage and current characteristics of a user-defined PV module type, operating under the temperature and solar radiation conditions of interest. The control unit design using an FPGA has the advantage of flexibility in case of changes, because of the reprogramming capability of reconfigurable logic, thus enabling the simulation of various PV module types. The FPGA devices are characterized by fast computation capability and provide the feasibility to implement parallel architectures, resulting in reduction of the control algorithm execution time [14,15]. Compared to the processor-based PV simulator implementations, using the proposed methodology enhances the rapid system prototyping capability, since the same VHDL source code which is used to configure the FPGA device for the real-time operation of the developed PV simulator can also be input to the appropriate simulation program in order to simulate the control algorithm operation, for functional verification purposes, before the hardware prototype construction. Furthermore, the same VHDL source code can be synthesized to any FPGA device, or can be used for the development of a custom chip, providing flexibility and technology independence [16].

The switched-mode power converters contain inductors consisting of coils wound on ferrite cores, which are magnetic materials capable of operating at switching frequencies up to several hundreds of kHz with low losses. The power converter size is primarily determined by the inductor magnetic material size, which is inversely proportional to the converter switching frequency. Thus, it is essential to increase the switching frequency of the power converter PWM control signal in order to reduce the converter size. The proposed design method has the advantage that due to the high-frequency operational characteristics of the FPGA devices, a PWM control unit architecture can be implemented such that the switched-mode power converter switching frequency can be highly increased. Currently, most power converters operate at frequencies up to 500 kHz due to limitations of power semiconductor and magnetic material technology at both, high-frequency and power levels. However, converter operating frequencies in excess of 1 MHz at high power and efficiency levels can be achieved using the planar transformer technology. As analyzed in [17], the conventional microcontroller or DSP-based control units cannot support the aforementioned switching frequency levels with adequate PWM duty cycle resolution. The power converter control unit design based on FPGA devices enables the integration of all power converter control operations in a single IC, facilitating the reduction of the total system cost.

The proposed system can be easily extended such that the environmental conditions time-series, under which the simulated PV module operates, are either measured in real-time using solar irradiance and temperature sensors, or they are defined by the user and interfaced to the PV simulator in digital format through a PC output port.

The mathematical modeling of the PV modules operation is presented in Section 2, the proposed PV simulator design is described in Section 3 and the simulation and experimental results are analyzed in Sections 4 and 5, respectively.

2. Mathematical modeling of the PV modules operation

The equivalent circuit of a PV module, depicted in Fig. 1, is described by the following equation [18]:

$$I = I_{SC}\left[1 - \exp\left(\frac{V - V_{OC} + IR_S}{V_t}\right)\right] - \frac{V + IR_S}{R_P} \tag{1}$$

$$V_t = \frac{mkT}{q} \tag{2}$$

where I, V are the PV module output voltage and current, I_{SC} is the ideal PV module short-circuit current (A), V_{OC} is the ideal PV module open-circuit voltage (V), V_t is the thermal voltage (V), m is a nonideality factor, k is the Boltzmann constant, T is the absolute cell temperature (K), q is the electron charge and R_S, R_P are the series and parallel resistance, respectively, of the PV module.

The I–V characteristics of a commercially available PV module for various cell temperature and incident solar irradiance conditions are shown in Fig. 2(a and b), respectively. The short-circuit current, I_{SC}, is proportional to the solar irradiance, G (W/m^2), incident on the module, while the open-circuit voltage, V_{OC}, is usually considered to depend only on the PV module cell temperature, T_C (°C), thus neglecting the effect of the incident solar irradiance on the open-circuit voltage:

$$I_{SC} = I_{SC,STC}\frac{G}{1000\ \mathrm{W/m^2}} \tag{3}$$

$$V_{OC} = V_{OC,STC} - k_T(T_C - 25\,^{\circ}\mathrm{C}) \tag{4}$$

$$T_C = T - 273\,\mathrm{K} = T_A + \frac{\mathrm{NOCT} - 20\,^{\circ}\mathrm{C}}{800\ \mathrm{W/m^2}}G \tag{5}$$

where $I_{SC,STC}$ is the short-circuit current (A) under standard test conditions (STC, cell temperature = 25 °C and solar irradiance = 1 kW/m^2), $V_{OC,STC}$ is the open-circuit voltage (V) under STC, k_T is the open-circuit voltage temperature coefficient (V/°C), T_C is the cell temperature (°C), T_A is the ambient temperature (°C) and NOCT is the normal operating cell temperature (°C).

The values of $I_{SC,STC}$, $V_{OC,STC}$, k_T and NOCT are specified by the PV module manufacturer. The effect of the cell temperature on the short-circuit current is assumed negligible.

The effect of the parallel resistance, R_P, is usually neglected, resulting in the following, simplified, I–V characteristic equation:

$$I = I_{SC}\left[1 - \exp\left(\frac{V - V_{OC} + IR_S}{V_t}\right)\right] \tag{6}$$

The PV module mathematical modeling presented above, has the drawback that the output current, I, appears on both sides of Eqs. (1) and (6). In order to avoid the corresponding calculation complexity, in this paper, the ideal PV module output current is calculated as follows:

$$I = I_{SC}\left[1 - \exp\left(\frac{V_S - V_{OC}}{V_t}\right)\right] = I_{SC}\left\{1 - \exp\left[C(T)\left(\frac{V_S}{V_{OC}} - 1\right)\right]\right\} \tag{7}$$

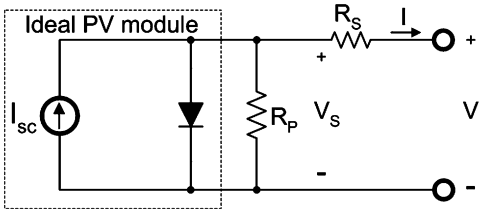

Fig. 1. The PV module equivalent circuit.

Please cite this article as: E. Koutroulis, et al., Development of an FPGA-based system for real-time simulation of photovoltaic modules, Microelectron. J (2008), doi:10.1016/j.mejo.2008.05.014

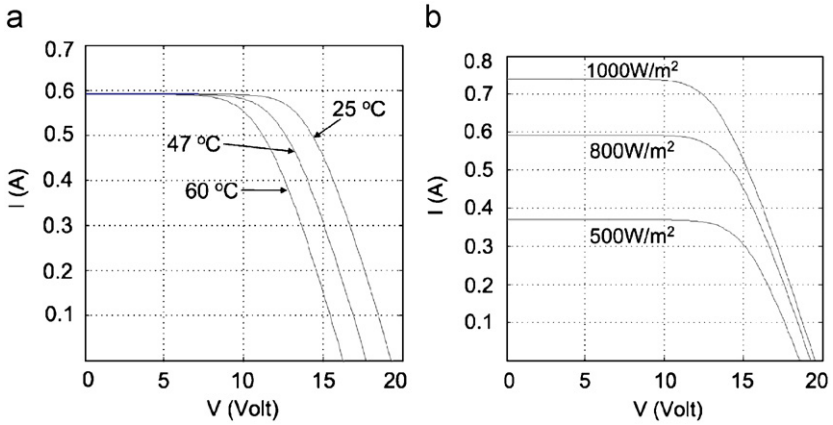

Fig. 2. The current–voltage characteristics of a PV module with temperature and incident irradiance: (a) constant irradiance and varying cell temperature and (b) constant cell temperature and varying irradiance.

$$C(T) = \frac{V_{OC}}{V_t} \tag{8}$$

$$0 \leqslant V_S \leqslant V_{OC} \tag{9}$$

where V_S is the ideal PV module output voltage.

Using the values of I calculated using Eq. (7), the corresponding values of the PV module output voltage, V, are calculated using the following equation:

$$V = V_S - IR_S \tag{10}$$

$$0 \leqslant V \leqslant V_{OC} \tag{11}$$

Considering the values of V_{OC} and V_t for various commercially available PV modules, operating under the temperature conditions of typical PV energy production applications, the temperature sensitivity of $C(T)$ in Eq. (7) is neglected in the proposed method. The simulation results indicate that the average absolute error of the ideal PV module output current values, calculated using this approach, is less than 1.8% of the short-circuit current. The ideal PV module modeling based on this approximation has the advantage of reduced calculation complexity. This is beneficial in case that the resulting, normalized I–V characteristic of the ideal PV module is stored in a look-up-table (LUT), which is part of a digital control system with limited availability of hardware resources, as analyzed in the next section.

3. Description of the proposed photovoltaic simulator

As illustrated in Fig. 3, the proposed PV simulator is composed of two subsystems:

(i) the switched-mode DC/DC power converter and
(ii) the control system, consisting of the FPGA unit, the analog to digital (A/D) converters and the voltage and current sensors.

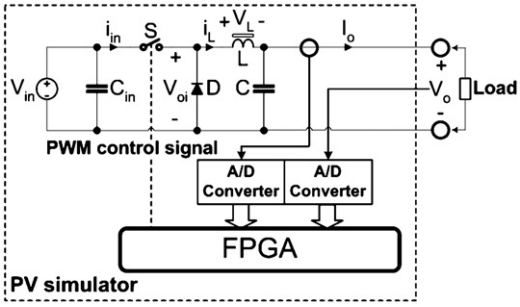

Fig. 3. The block diagram of the proposed PV simulator.

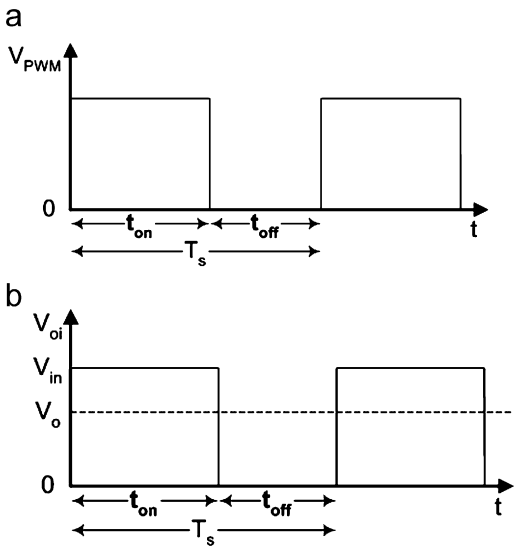

Fig. 4. The DC/DC converter principal waveforms.

The power converter input voltage, V_{in}, is an unregulated DC voltage. A constant frequency PWM control signal, V_{PWM}, depicted in Fig. 4(a), is produced by the FPGA unit and it is used to control the power switch, S, in order to modulate the DC input voltage into a high-frequency wave, V_{oi}, shown in Fig. 4(b), which then passes through a lowpass L-C filter producing the DC output voltage, V_O. The DC output voltage is regulated to the desired value by adjusting the PWM signal duty cycle value, D, as follows:

$$V_O = DV_{in} = \frac{t_{on}}{T_S} V_{in} \tag{12}$$

where t_{on} is the PWM signal ON time and T_S is the switching period.

The inductor, L, is wound on a ferrite core and its value is selected such that the converter operates in the continuous

Please cite this article as: E. Koutroulis, et al., Development of an FPGA-based system for real-time simulation of photovoltaic modules, Microelectron. J (2008), doi:10.1016/j.mejo.2008.05.014

conduction mode [19]. The simulator DC output voltage is measured using a voltage divider, while the DC output current is measured using a current shunt sensor. Both sensors are connected to op-amp-based voltage-follower circuits. The resulting output voltage and current measurements are interfaced in digital format to the FPGA unit through the corresponding 8-bit A/D converters.

The DC/DC converter output voltage and current are related, in case of ohmic load, according to the linear characteristic displayed in Fig. 5. The simulated PV module *I–V* characteristic, which is calculated by the control circuit implemented in the FPGA unit, is also indicated in the figure. Depending on the PWM control signal duty cycle value, the DC/DC converter output voltage is successively regulated, such that the converter operates at points A_1, A_2, etc. At each operating point, the PV simulator output current, I_{act}, is compared with the corresponding PV module current, I_{th} and their difference is used by the control unit in order to adjust the PWM signal duty cycle value until convergence to the operating point A_k has been achieved. At this operating point, the difference of the simulated and actual currents is zero, thus the PV simulator output voltage and current are equal to the corresponding values of the simulated PV module.

The block diagram of the control unit hardware implemented in the FPGA IC is depicted in Fig. 6. The calculated parameters word length selection is a compromise between the target FPGA device capacity and clock speed specifications and the PV simulator accuracy requirements. Increasing the calculated parameters word length results in higher PV simulator accuracy. However, the PV simulator cost is increased in such a case since the number of FPGA device logic cells required for the implementation of the corresponding control arithmetic is also higher. The control unit design presented in this section is based on an 8-bit PWM signal duty cycle resolution resulting in acceptable accuracy and low FPGA device cost, but it can be easily modified to fulfill the desired PV simulator accuracy and cost specifications.

The *I–V* characteristic of an ideal PV module, described by Eq. (7), is quantized in 8-bit integer format using the following relations:

$$V_{I8m} = V_S \frac{(2^8 - 1)}{V_{OC,STC} - k_T(T_{C,ref} - 25\,^\circ\mathrm{C})} \tag{13}$$

$$I_{I8m} = I \frac{2^8 - 1}{I_{SC,STC}(G_{ref}/1000\,\mathrm{W/m^2})} \tag{14}$$

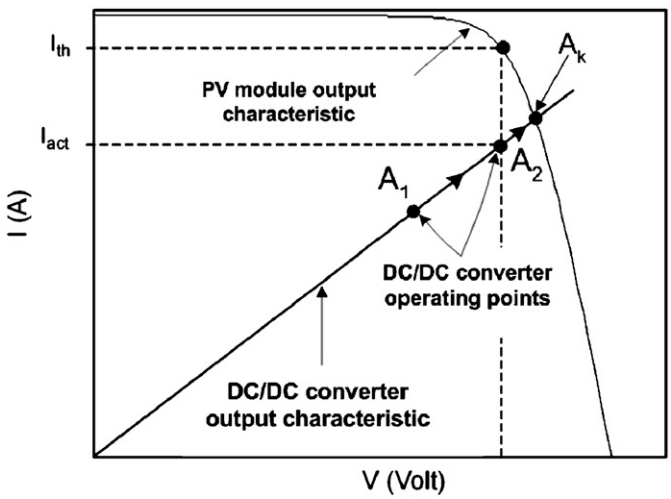

Fig. 5. The proposed PV simulator control method.

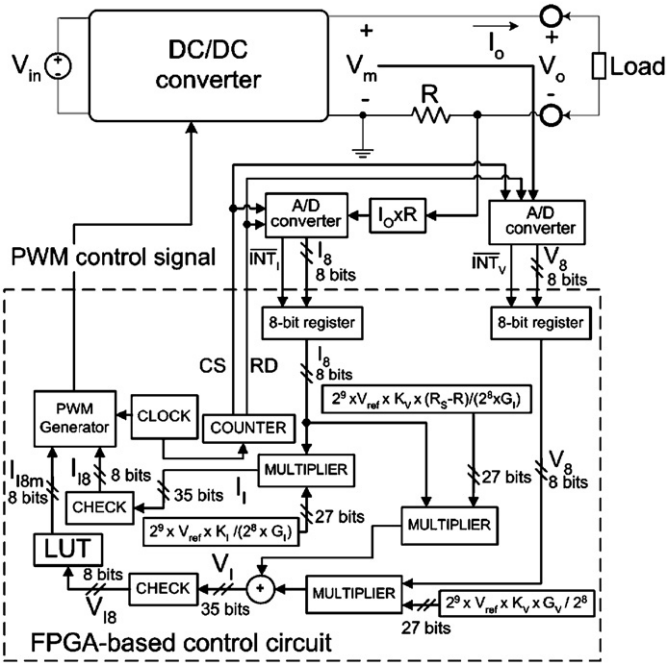

Fig. 6. The control unit hardware implementation.

where V_{I8m} and I_{I8m} are the resulting integer values of the ideal PV module voltage and current, respectively and G_{ref}, $T_{C,ref}$ are the simulated PV module reference incident solar irradiance and cell temperature operating conditions, which are used to develop the ideal PV module normalized *I–V* characteristic stored in the LUT.

The value of $T_{C,ref}$ is selected according to the simulated PV module operating temperature range such that the error arising due to the inherent constant $C(T)$ value approximation is minimized, while the value of G_{ref} is selected according to the I_{I8m} resolution requirements. The resulting V_{I8m} and I_{I8m} pairs are stored in an LUT, implemented in the FPGA unit. Using the ideal PV module normalized *I–V* characteristic stored in the LUT, the corresponding characteristic of the simulated PV module can be calculated for any cell temperature and incident solar irradiance operating conditions, defined by the PV simulator operator.

The DC/DC converter measured output voltage, V_m, and current, I_O, are converted to digital form using the corresponding A/D converters and the resulting 8-bit integer values, V_8 and I_8, respectively, can be calculated as follows:

$$V_8 = \frac{V_m 2^8}{G_V V_{ref}} \tag{15}$$

$$I_8 = \frac{I_O G_I 2^8}{V_{ref}} \tag{16}$$

where G_V and G_I are the voltage and current sensor gains and V_{ref} is the reference voltage of the A/D converters.

The RD and CS signals are used to control the A/D converter operation, in order to measure the parameters V_8 and I_8 with the desired sampling rate, f_{sa}. The current and voltage samples produced are output from the corresponding 8-bit registers when the A/D end-of-conversion signals, $\overline{INT_I}$ and $\overline{INT_V}$, respectively, are activated.

When convergence to the operating point A_k has been achieved, the output voltage of the ideal PV module, V_S, which is stored in digital format in the LUT, is related with V_m

and I_O, as follows:

$$V_S = V_m + I_O R_S - I_O R \tag{17}$$

where R is the current sensor resistance value.

Since all physical parameters defining the PV simulator operation are real numbers, their values are multiplied with a power of two, taking into account, both (a) the available hardware resources and (b) the precision requirements. Thus, the precision of the calculations is increased and both the multiplication and the division functions can be implemented by applying bit-shifting operators. Using Eqs. (15)–(17), the ideal PV module voltage is calculated in 35-bit integer format, V_I, using the following relationship:

$$V_I = \frac{2^9 K_V G_V V_{ref} V_8}{2^8} + \frac{2^9 K_V I_8 V_{ref}(R_S - R)}{2^8 G_I} \tag{18}$$

$$K_V = \frac{(2^8 - 1)}{V_{OC,STC} - k_T(T_C - 25\,^\circ\mathrm{C})} \tag{19}$$

where T_C is the desired cell temperature of the simulated PV module, defined by the PV simulator operator.

The result of the above calculation is used in order to retrieve the corresponding value of the ideal PV module output current, stored in the LUT. The ideal PV module I–V characteristic has been stored in the LUT in 8-bit integer format, while V_I must be implemented as a 35-bit integer such that the corresponding value calculated using Eq. (18) has adequate precision. Thus, the function "check", depicted in the diagram shown in Fig. 6, is used to shift right by 9 bits the value of V_I and then examine the status of the 9th to the 35th resulting bits. If any of these bits is in logical '1' state then the value of the number under examination is larger than the maximum value stored in the LUT and it corresponds to a voltage value larger than the open-circuit voltage of the simulated PV module. In such a case, the value input to the LUT is set equal to 255.

The parameter I_8, corresponding to the PV simulator output current, is also scaled, in order to compensate the attenuations of the current sensor and the A/D converter modules, using the following relationship:

$$I_I = \frac{2^9 I_8 V_{ref} K_I}{2^8 G_I} \tag{20}$$

$$K_I = \frac{2^8 - 1}{I_{SC,STC}(G/1000\,\mathrm{W/m^2})} \tag{21}$$

where I_I is the resulting 35-bit value and G is the desired incident solar irradiance of the simulated PV module, defined by the PV simulator operator.

The function "check" is also applied to the result of this calculation.

The PWM signal duty cycle value is calculated by comparing I_{I8m} and I_{I8}, according to the following control law:

$$D_k = D_{k-1} + \Delta D_{k-1} = D_{k-1} + C\,\mathrm{sign}\,(I_{I8m} - I_{I8}) \tag{22}$$

where D_k is the 8-bit duty cycle value at step k, C is a constant determining the speed and accuracy of convergence to the PV module target operating point and the function sign(x) is defined as

$$\begin{aligned} &\mathrm{sign}\,(x) = 1 \quad \text{if } x \geqslant 0, \\ &\mathrm{sign}\,(x) = -1 \quad \text{if } x < 0. \end{aligned} \tag{23}$$

Using the calculated PWM signal duty cycle value, D_k, the PWM signal is produced by the PWM generation unit, displayed in Fig. 7.

The value of D_k is compared with the output of an 8-bit free-running counter. When they are equal, the R input of the RS flip-flop is set to logical '1' state. The overflow signal of the counter is connected to the S input of the flip-flop and the frequency of the PWM switching signal which is produced, f_{PWM}, is related to the system clock frequency, f_{clock}, as follows:

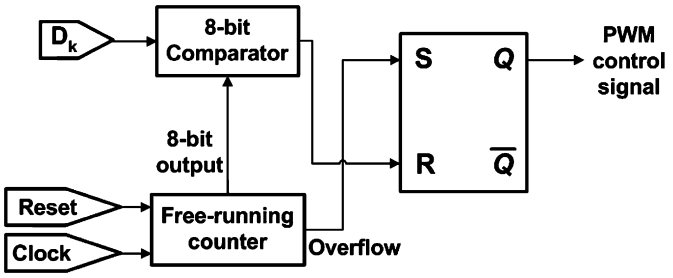

Fig. 7. The PWM generator unit block diagram.

$$f_{PWM} = \frac{f_{clock}}{2^8} \tag{24}$$

4. Simulation results

The functional verification of the FPGA-based control unit architecture presented in the previous section was accomplished using a software program developed according to the VHDL language and the ModelSim v6.0 simulation platform. The values of the control logic inputs $\overline{INT_I}$, $\overline{INT_V}$, I_8 and V_8 were manually adjusted by the simulation software operator during the simulation process. The simulated timing waveforms of the CS, RD, $\overline{INT_I}$, $\overline{INT_V}$ and PWM signals are depicted in Fig. 8. The binary values of the current and voltage samples input to the control unit have been set to $I_8 = 11000111$ and $V_8 = 10011011$, respectively. The PV simulator output current and voltage sampling is performed at the time instant t_1. At the time instant t_2 the end-of-conversion signals $\overline{INT_I}$ and $\overline{INT_V}$ are activated and the corresponding current and voltage samples, I_8 and V_8, are input to the FPGA-based control logic. Then, the PWM control signal duty cycle, having an initial value of $D = 77.73\%$, is updated to its new value $D = 89.84\%$ according to the control algorithm computations presented in the previous section. This simulation process was repeated for various combinations of current and voltage samples input to the FPGA-based control logic in order to verify the correct operation of both the control architecture and the corresponding VHDL program code.

The developed architecture has been synthesized for various target FPGA devices using the aforementioned VHDL program code and the Xilinx Foundation software v4.1. The post-layout results of the device resources required to implement the control unit of the proposed system together with the corresponding cost are displayed in Table 1. It is observed that the implementation of the proposed architecture occupies a relatively small percentage of the corresponding device logic cells, thus permitting the integration of additional, more complex, power converter control operations in the same IC and the implementation of the proposed control arithmetic with more bits, thus increasing the PV simulator accuracy. The FPGA device type is selected according to the PV simulator control unit implementation area and cost requirements.

The resulting post-layout maximum PWM signal frequency achieved using the proposed architecture for various FPGA devices, is shown in Table 1. The corresponding maximum current and voltage sampling frequency achieved is also indicated in this table. It is observed that using the proposed FPGA-based

Please cite this article as: E. Koutroulis, et al., Development of an FPGA-based system for real-time simulation of photovoltaic modules, Microelectron. J (2008), doi:10.1016/j.mejo.2008.05.014

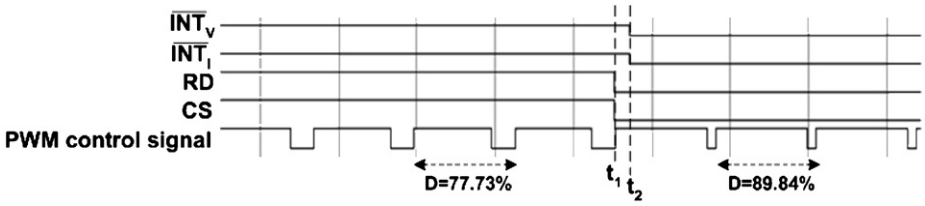

Fig. 8. The simulated timing waveforms of the principal control signals.

Table 1
Post-layout results for various FPGA devices

FPGA device type	Device resources required (logic cells)	Maximum PWM signal frequency (kHz)	Maximum sampling frequency (kHz)	Cost ($)
Virtex XC2V1000	888 out of 27,648 (3%)	313.50	78.37	252.0
Spartan-3 XCES50	476 out of 1728 (27.5%)	111.54	27.88	288.0
Spartan-3 XC3S400	412 out of 8064 (5%)	132.49	33.12	30.0
Virtex-4 4VLX80FF1148-11	1000 out of 80,640 (1.2%)	246.20	61.55	72.0
Spartan-3 XC3S1000	LUTs: 1708 out of 15,360 (11%)	286.84	71.71	20.00

architecture PWM frequencies in excess of 100 kHz can be achieved at relatively low cost. The maximum PWM frequency produced by commercially available DSP or microcontroller devices with on-chip PWM generation units is less than 100 kHz, even if the corresponding clock speed is of the order of 400 MHz. Under practical conditions the maximum PWM signal frequency that can be achieved using the proposed methodology can be considerably higher compared to the simulated timing analysis results presented above, since the timing analyzer is rather conservative. Thus, the post-layout timing results are frequently used to analyze and demonstrate the performance of FPGA designs. Additionally, the maximum PWM signal frequency can be further increased using manual placement techniques during the FPGA device configuration stage.

5. Experimental results

A prototype PV simulator has been developed using the above-described methodology and tested in the laboratory. The DC/DC converter power switch, S, consists of an IRFZ44 MOSFET rated at 60 V, 50 A, while the flyback diode, D, has a 35 ns reverse-recovery time. The input and output capacitor values are $C_{in} = 470\,\mu F$ and $C = 4700\,\mu F$, respectively. The output inductor value is $L = 4\,mH$. The proposed architecture operation was verified using the XS40 v1.2 board, which contains the Xilinx 4010XLPC84-3 FPGA IC. The on-board clock running at 12 MHz was used and the resulting PWM frequency was 46.875 kHz, while the PV simulator output voltage and current sampling rate is equal to 11.7 kHz. The selected PWM frequency is relatively low compared to the target switching frequency of the proposed design, analyzed in Section 1, since a low cost system with a low clock frequency generator was used only for functional verification of the proposed architecture. However, by selecting the appropriate FPGA device type and the corresponding clock frequency generator, the proposed system performance at the higher PWM switching frequency levels presented in the previous section can be achieved under any practical conditions, due to the high accuracy of the post-layout timing analysis results.

The operation of a commercially available PV module, operating under various temperature and irradiance conditions, was simulated using several DC/DC converter input voltage values. The values of cell temperature and incident solar irradiance of interest were input to the developed program code before the synthesis process. In order to evaluate the accuracy of the developed PV simulator, the percentage deviation, $\varepsilon(\%)$, of the theoretical and experimental output current values, corresponding to the same PV output voltage, has been calculated using the following equation:

$$\varepsilon(\%) = \frac{|I_{theoretical} - I_{measured}|}{I_{theoretical}} 100\% \quad (25)$$

where $I_{theoretical}$ is the output current (A) of the simulated PV module and $I_{measured}$ is the proposed simulator output current (A), both corresponding to the same output voltage. The theoretical I–V characteristics have been calculated according to the PV module modeling described by Eqs. (7)–(11), using the exact values of $C(T)$. The $C(T)$ value approximation approach has only been used to develop the LUT stored in the FPGA-based control unit, in order to reduce the FPGA device hardware resources required.

The I–V characteristic of the simulated PV module operating at a solar irradiance level of 800 W/m^2 and 45 °C temperature is shown in Fig. 9(a). The corresponding operating points of the developed PV simulator, in case that the DC input voltage is 30 V, are also indicated in the figure. The values of $\varepsilon(\%)$ are depicted in Fig. 9(b), having an average value of 1.28%. The corresponding results in case that the DC/DC converter input voltage is increased to 35 V are shown in Fig. 10. The average current deviation in this case is 0.8%. The theoretical I–V characteristic and the PV simulator operating points, in case that the simulated PV module operates under 1000 W/m^2 solar irradiance and 25 °C temperature, are shown in Fig. 11(a). The DC/DC converter input voltage is 36.4 V in this case. The current deviation, $\varepsilon(\%)$, depicted in Fig. 11(b), has an average value of 0.73%. The corresponding results, in case that the simulated PV module cell temperature is increased to 47 °C, are presented in Fig. 12. The average current deviation in this case is 1.12%. The theoretical and experimental results in case that the simulated PV module operates under 800 W/m^2 solar irradiance and 45 °C temperature, while the power converter DC input voltage value is 36.4 V, are depicted in Fig. 13. The average percentage deviation between the theoretical and experimental output current values is 1.25%. It is observed that the PV simulator output voltage and current do not appreciably depend on the power converter input

Please cite this article as: E. Koutroulis, et al., Development of an FPGA-based system for real-time simulation of photovoltaic modules, Microelectron. J (2008), doi:10.1016/j.mejo.2008.05.014

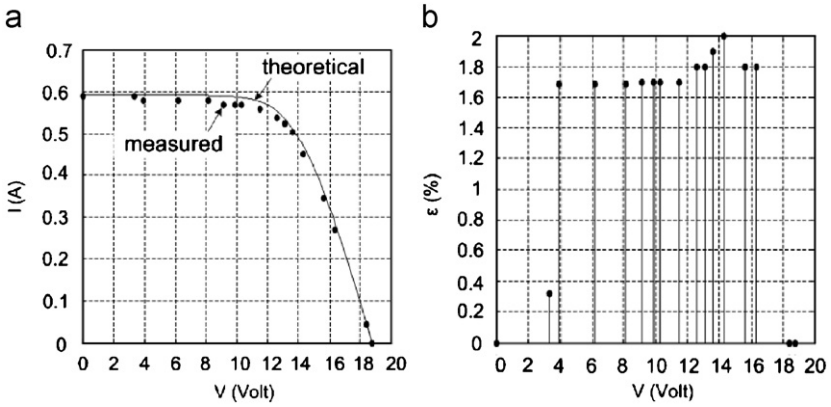

Fig. 9. (a) The theoretical and experimental results in case of $V_{in} = 30$ V, while the simulated PV module operates under 800 W/m^2, 45 °C and (b) the corresponding values of $\varepsilon(\%)$.

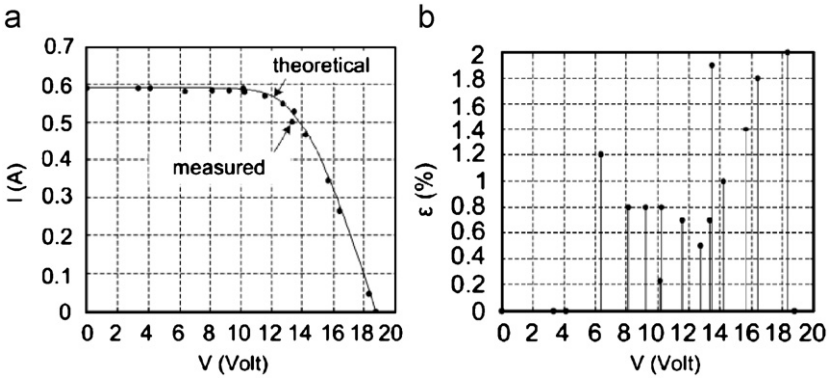

Fig. 10. (a) The theoretical and experimental results in case of $V_{in} = 35$ V, while the simulated PV module operates under 800 W/m^2, 45 °C and (b) the corresponding values of $\varepsilon(\%)$.

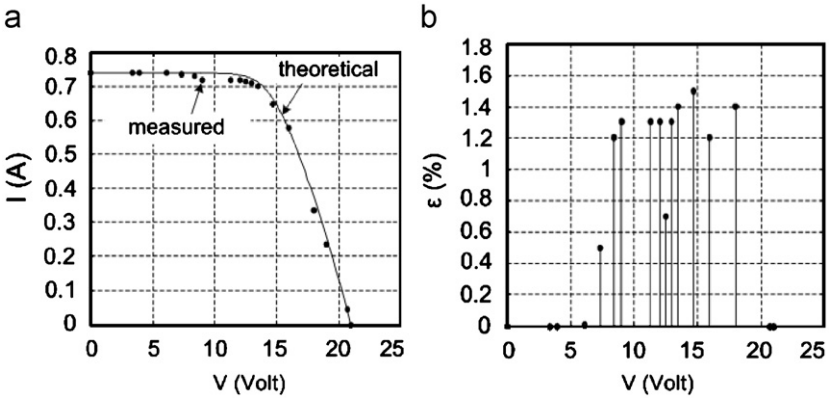

Fig. 11. (a) The theoretical and experimental results in case of $V_{in} = 36.4$ V, while the simulated PV module operates under 1000 W/m^2, 25 °C and (b) the corresponding values of $\varepsilon(\%)$.

voltage, thus indicating the line-regulation capability of the developed system. The proposed PV simulator operation has been measured under additional input voltage and simulated PV module environmental operating conditions and the average value of the current deviation has been calculated to be approximately 1.03%.

The proposed PV simulator has been used to simulate the operation of a commercially available PV module. The output power capability of the PV simulator can be increased by using a DC/DC converter of higher power rating. In case of power switches (MOSFET, IGBT, etc.) operating power limitations at high switching frequency levels, the output power capability of a high switching frequency PV simulator can be increased by using multiple low power, high switching frequency DC/DC converter modules operating in parallel. In both cases the FPGA-based control unit architecture presented in the subject paper is not required to be modified since its operation depends only on the relationship between the output current and voltage of the simulated PV module and not on the DC/DC converter power capability.

Please cite this article as: E. Koutroulis, et al., Development of an FPGA-based system for real-time simulation of photovoltaic modules, Microelectron. J (2008), doi:10.1016/j.mejo.2008.05.014

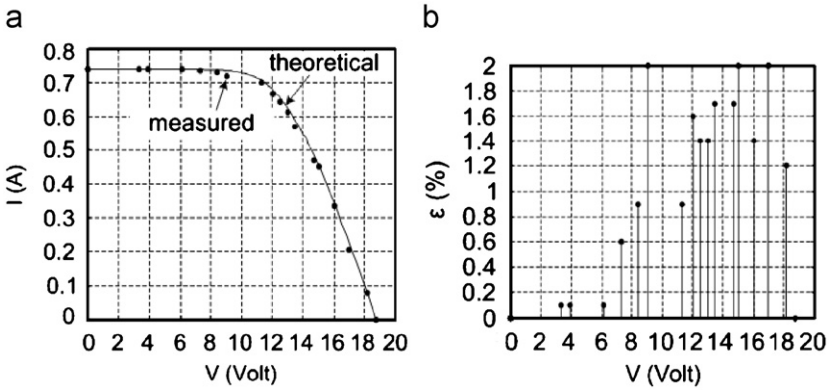

Fig. 12. (a) The theoretical and experimental results in case of $V_{in} = 36.4\,V$, while the simulated PV module operates under $1000\,W/m^2$, 47 °C and (b) the corresponding values of $\varepsilon(\%)$.

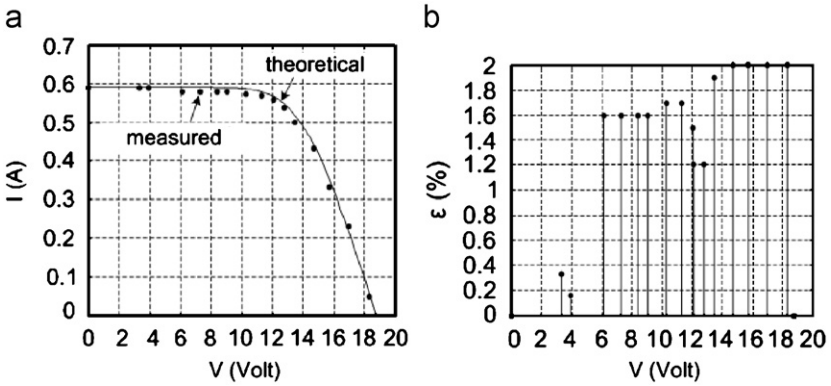

Fig. 13. (a) The theoretical and experimental results in case of $V_{in} = 36.4\,V$, while the simulated PV module operates under $800\,W/m^2$, 45 °C and (b) the corresponding values of $\varepsilon(\%)$.

6. Conclusions

PV simulators are indispensable for the operational evaluation of PV energy production system components (e.g. battery chargers, DC/AC inverters, etc.) in order to avoid the time-consuming and expensive field-testing process. In this paper, the development of a novel real-time PV simulator based on FPGA ICs, has been presented. The system operator is able to define both the PV module type to be simulated and the environmental conditions under which the selected PV module operates. The proposed design method has the advantage of enhancing the rapid system prototyping capability, while due to the high-frequency operational characteristic of the FPGA-based control unit, the switched-mode power converter switching frequency can be highly increased, resulting in substantial power converter size and cost reduction. The experimental results indicate that, using the proposed method, the PV module *I–V* characteristics examined are reproduced with an average accuracy of 1.03%.

The proposed system can be easily extended such that the environmental conditions time-series, under which the simulated PV module operates, are either measured in real-time using solar irradiance and temperature sensors, or they are defined by the user and interfaced to the PV simulator in digital format through a PC output port.

Acknowledgment

The assistance of Prof. Apostolos Dollas during the development of the FPGA-based control unit is acknowledged.

References

[1] H. Matsukawa, K. Koshiishi, H. Koizumi, K. Kurokawa, M. Hamada, L. Bo, Dynamic evaluation of maximum power point tracking operation with PV array simulator, Sol. Energy Mater. Sol. Cells 75 (2003) 537–546.
[2] K. Khouzam, K. Hoffman, Real-time simulation of photovoltaic modules, Sol. Energy 56 (1996) 521–526.
[3] A.K. Mukerjee, N. Dasgupta, DC power supply used as photovoltaic simulator for testing MPPT algorithms, Renewable Energy 32 (2007) 587–592.
[4] S. Armstrong, C.K. Lee, W.G. Hurley, Investigation of the harmonic response of a photovoltaic system with a solar emulator, in: European Conference on Power Electronics and Applications, 2005, pp. 1–8.
[5] H. Nagayoshi, *I–V* curve simulation by multi-module simulator using *I–V* magnifier circuit, Sol. Energy Mater. Sol. Cells 82 (2004) 159–167.
[6] S.H. Lloyd, G.A. Smith, D.G. Infield, Design and construction of a modular electronic photovoltaic simulator, in: International Conference on Power Electronics and Variable Speed Drives, 2000, pp. 120–123.
[7] A. Luiz, C. Lopes, Anne-Marie Lienhardt, A simplified nonlinear power source for simulating PV panels, in: IEEE 34th Annual Power Electronics Specialists Conference, vol. 4, 2003, pp. 1729–1734.
[8] T. Easwarakhanthan, J. Bottin, A. El-Slassi, R. Ravelet, S. Ravelet, Micro-computer-controlled simulator of a photovoltaic generator using a programmable voltage generator, Sol. Cells 17 (1986) 383–390.
[9] G. Vachtsevanos, K. Kalaitzakis, A hybrid photovoltaic simulator for utility interactive studies, IEEE Trans. Energy Convers. 2 (1987) 227–231.
[10] Dexin Li, Pai H. Chou, Maximizing efficiency of solar-powered systems by load matching, in: Proceedings of the 2004 International Symposium on Low Power Electronics and Design, 2004, pp. 162–167.
[11] Q. Zeng, P. Song, L. Chang, A photovoltaic simulator based on DC Chopper, in: Proceedings of the 2002 IEEE Canadian Conference on Electrical and Computer Engineering, vol. 1, 2002, pp. 257–261.
[12] S.S. Kulkarni, C.Y. Thean, A.W. Kong, A novel PC based solar electric panel simulator, in: Fifth International Conference on Power Electronics and Drive Systems, vol. 2, 2003, pp. 848–852.
[13] P. Sanchis, J. Lopez, A. Ursua, L. Marroyo, Electronic controlled device for the analysis and design of photovoltaic systems, IEEE Power Electron. Lett. 3 (2005) 57–62.

Please cite this article as: E. Koutroulis, et al., Development of an FPGA-based system for real-time simulation of photovoltaic modules, Microelectron. J (2008), doi:10.1016/j.mejo.2008.05.014

[14] M. Naouar, E. Monmasson, A.A. Naassani, I.S. Belkhodja, N. Patin, FPGA-based current controllers for AC machine drives—a review, IEEE Trans. Ind. Electron. 54 (2007) 1907–1925.
[15] C. Paiz, M. Porrmann, The utilization of reconfigurable hardware to implement digital controllers: a review, in: IEEE International Symposium on Industrial Electronics, 2007, pp. 2380–2385.
[16] A. Castro, P. Zumel, O. Garcia, T. Riesgo, J. Uceda, Concurrent and simple digital controller of an AC/DC converter with power factor correction based on an FPGA, IEEE Trans. Power Electron. 18 (2003) 334–343.
[17] E. Koutroulis, A. Dollas, K. Kalaitzakis, High-frequency pulse width modulation implementation using FPGA and CPLD ICs, J. Systems Architecture 52 (2006) 332–344.
[18] E. Lorenzo, Solar Electricity: Engineering of Photovoltaic Systems, Progensa, 1994.
[19] N. Mohan, T. Undeland, W. Robbins, Power Electronics: Converters, Applications and Design, second ed., Wiley, New York, 1995.

Please cite this article as: E. Koutroulis, et al., Development of an FPGA-based system for real-time simulation of photovoltaic modules, Microelectron. J (2008), doi:10.1016/j.mejo.2008.05.014